

Quantum size effect in self-organized InAs/GaAs quantum dots

R. Heitz,¹ O. Stier,¹ I. Mukhametzhanov,² A. Madhukar,² and D. Bimberg¹

¹*Institut für Festkörperphysik, Technische Universität Berlin, Sekr. PN 5-2, Hardenbergstraße 36, D-10623 Berlin, Germany*

²*Photonic Materials and Devices Laboratory, Departments of Physics and Materials Science, University of Southern California,*

Los Angeles, California 90089

(Received 17 March 2000)

The quantum size effect of exciton transitions is investigated experimentally and theoretically for self-organized InAs/GaAs quantum dots (QD's). Photoluminescence excitation (PLE) experiments are reported for a series of samples with QD's varying in average size, revealing size-dependent excitation resonances. Temperature-dependent measurements show that the PLE spectra mirror the absorption spectra of QD's with a certain ground state transition energy. The observed PLE resonances are identified based on their energy, relative intensity, and sensitivity to size variations in comparison to results of eight-band $\mathbf{k} \cdot \mathbf{p}$ calculations for pyramidal InAs/GaAs QD's with {101} side facets. Band mixing, strain, and the particular geometry of the three-dimensional confinement lead to a rich fine structure with a variety of "forbidden" excitonic transitions. A good agreement between experiment and theory is found for large QD's ($E_{\text{det}} \leq 1.1$ eV), whereas the agreement becomes worse for smaller QD's. The discrepancies arise, most likely, from the uncertainties in the size- and growth-dependent variations of the QD shape and composition as well as Coulomb-induced localized wetting layer states.

I. INTRODUCTION

The effect of quantum confinement on the electronic states in semiconductor nanostructures has been studied for decades. In 1974 Dingle, Wiegman, and Henry¹ demonstrated the quantum-size effect for one-dimensional confinement in quantum well structures, an effect that is textbook knowledge nowadays. Subsequently, this effect has been demonstrated also for three-dimensional confinement in highly symmetric systems like colloidal II-VI and III-V quantum dots (QD's) (Refs. 2 and 3) or QD's made from quantum wells by exploiting modern etching techniques,⁴ local interdiffusion,⁵ or the strain fields of self-organized nanostressors.⁶ Only limited information is, however, available on the details and the quantum-size effect of the electronic structure of self-organized epitaxial island QD's.⁷

The potential of self-organized island formation during highly strained epitaxy to produce small coherently embedded QD's with large energy level separations has stimulated considerable research on zero-dimensional (0D) systems in recent years.⁷ The self-organized growth affords, however, only limited control on the structural properties and thus on the discrete energy spectrum of such QD's. The average size of the QD's might be modified in a limited way by the InAs deposition amount,⁸⁻¹⁰ the growth procedure,¹⁰ or applying an optically inactive seed layer fixing the island density.^{11,12} A large variety of different shapes have been reported for InAs/GaAs QD's by various groups, ranging from a pronounced pyramidal shape or less pointed dome shape with side facets oriented along {101},¹³ {105},¹⁴ {113},¹⁵ {114},^{8,16} or {136},¹⁷ to rather flat disklike structures.¹⁸ Obviously, the structural properties of the islands, which are crucial for the electronic properties, depend on the details of the growth conditions, deposition amount, and procedure. Optical data^{19,20} suggested an increase of the average height-to-width aspect ratio with increasing island size. Recent atomic force

microscopy (AFM) data have shown¹⁰ a change in the aspect ratio at a self-limiting base size with increasing island volume.

Photoluminescence (PL) spectroscopy at high excitation densities, taking advantage of state filling in the discrete density of states, is the most common experimental access to excited exciton states in such QD's.^{6,19,21-23} However, such measurements are restricted by the inhomogeneous broadening of the QD ensemble and, in addition, probe the spectrum of highly populated QD's, which is subject to many-particle effects.²⁴ The nearly equidistant series of excited state transitions found in such experiments suggested an interpretation in terms of "allowed" transitions ($\Delta n=0$) in a two-dimensional harmonic oscillator potential.^{6,21,22} Such models are, however, inherently unable to account for the characteristic peculiarities of self-organized QD's, i.e., the complex shape and the inhomogeneous strain.

Recently, more detailed calculations of the electronic structure of strained InAs/GaAs QD's using eight-band $\mathbf{k} \cdot \mathbf{p}$ theory^{25,26} or empirical pseudopotential (EP) theory²⁷ became available. These calculations predict nonequidistant energy levels, the complete removal of orbital degeneracy, and the breakdown of the stringent selection rules for dipole transitions. An essential role is played by the lowering of the QD symmetry to C_{2v} due to the piezoelectric effect induced by shear strain and due to the atomistic inequivalency of (110) and (1 $\bar{1}$ 0) directions.²⁷

The experimental verification of such calculations requires overcoming the inhomogeneous broadening in the optical spectra and probing the absorption spectrum of empty QD's. The inhomogeneity is avoided in single-QD spectroscopy,²⁸⁻³⁵ which is thus the ultimate tool in studying the rich fine structure in the excited state spectrum of localized excitons. The comparison with calculations is, however, hampered by the practically unknown structural properties of the actually investigated single QD. Alternatively, photolu-

minescence excitation (PLE) spectroscopy on a QD *ensemble* probes the absorption of a subensemble of *similar* QD's defined by the detection energy. Such spectra are still inhomogeneously broadened due to shape and composition variations but allow us to study the *size dependence* by tuning the detection window across the QD PL peak.^{20,36} Attention must, however, be paid to the possibility that restricted intradot relaxation^{37,38} might influence the shape of the PLE spectra. Multi-LO-phonon resonances have been reported for samples providing competing recombination processes which efficiently depopulate the excited QD states.^{39,40} Hence, both an excellent material quality and a high uniformity of the QD's are preconditions for a PLE study of the excited state spectrum.

In this paper we present a comprehensive study of the near-resonant PLE spectra for self-organized InAs/GaAs samples with different average QD sizes. Temperature-dependent measurements demonstrate that the observed PLE spectra indeed correspond to empty-dot absorption spectra and are a suitable tool to study the excited state transitions, giving access to the quantum-size effect. The experimental data are compared to single-exciton spectra calculated based on previously reported eight-band $\mathbf{k}\cdot\mathbf{p}$ single-particle states.²⁶ We find idealized InAs pyramids with $\{101\}$ side facets to be a good approximation for the large QD's (with a ground state transition energy $E_{\text{det}} \leq 1.1$ eV), whereas for smaller islands the level separations are systematically overestimated.

II. SAMPLE GROWTH AND EXPERIMENT

The investigated samples were grown by molecular beam epitaxy on semi-insulating GaAs(001) as described in detail in Refs. 11 and 36. Between 1.74 and 3.00 monolayers (ML) InAs were deposited at 500 °C, an As₄ partial pressure of 6×10^{-6} Torr, and a growth rate of 0.22 ML⁻¹. Immediately following the InAs deposition the substrate temperature was reduced to 400 °C for the growth of the GaAs cap layer using migration enhanced epitaxy. Such growth conditions combine a high barrier quality with an expected minimum of changes in the island shape and composition during overgrowth.^{20,36} In order to vary the structural properties of the QD ensembles two different growth approaches have been applied to the active layer. InAs was deposited either in the conventional continuous fashion³⁶ (C) or in the variable deposition amount (V) approach with a 1.74 ML InAs QD seed layer.¹¹ The latter method produces vertical pairs of differently sized QD's, in which for the used spacer thicknesses fast energy transfer processes render only the larger QD in the second layer optically active.^{11,12} The samples are dubbed C and V, respectively, followed by the amount of InAs deposited for the active layer given in percent of a ML (e.g., V300).

AFM measurements on equivalent uncapped samples show island densities between 300 and 900 μm^{-2} and average island heights ranging from 4 to 10 nm.⁹⁻¹¹ The island base length is systematically overestimated in AFM measurements but cross-sectional transmission electron microscopy (TEM) for an uncapped V300 sample indicates an average island base length of ~ 19 nm.⁴¹ Additionally, structural^{10,11} and optical^{19,20} studies suggest that along with

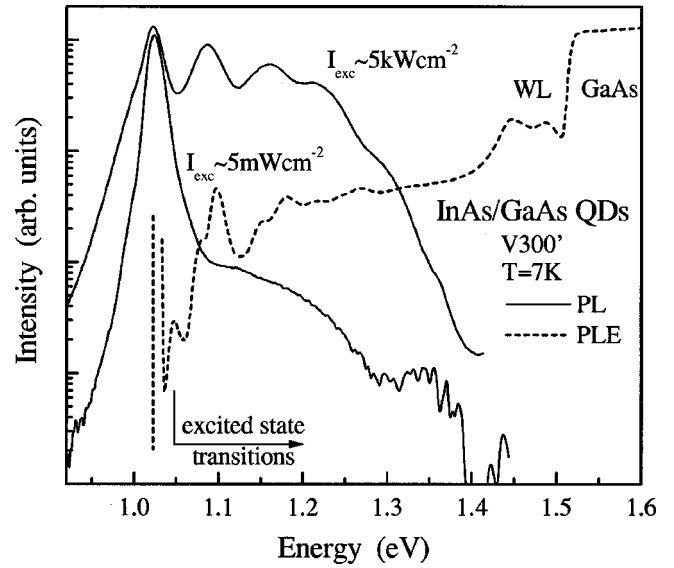


FIG. 1. PL and PLE spectra of the sample V300'. The FWHM of the ground state PL is 18 meV for an excitation density of $\sim 5 \text{ m W cm}^{-2}$.

the average QD size the ensemble uniformity and the average aspect ratio of the islands increase.

The optical measurements were performed in a continuous-flow He cryostat at temperatures between 5 and 250 K. The PL and PLE spectra were excited by an Ar⁺ laser or by a tungsten lamp dispersed by a 0.27 m double-grating monochromator as tunable light source providing an excitation area of $\sim 2 \text{ mm}^2$. The emission was spectrally dispersed by a 0.3 m double-grating monochromator and detected with a cooled Ge diode.

III. EXPERIMENTAL RESULTS

The PL of the investigated InAs/GaAs QD samples covers, at He temperatures and weak nonresonant excitation in the GaAs barrier, the energy range between 1.0 and 1.3 eV with peak energies between 1.023 and 1.18 eV, as reported previously.^{11,20,36,41} The average QD size in the samples was shown to depend on the growth mode and the InAs deposition amount: The smallest QD's were found^{20,36} in the continuously grown sample with 1.74 ML InAs deposition (i.e., C174) having a ground state transition energy of ~ 1.18 eV. Increasing the InAs deposition amount or applying a seed layer (in the variable deposition amount approach) increases the average island size, resulting in a redshift of the ground state PL. The lowest transition energy of ~ 1.02 eV is observed for the V300 samples, for which the controlled reduction of the lateral QD density by a medium-density seed layer enables the islands to grow to a base length of ~ 19 nm and a height of ~ 10 nm.^{10,41} The room-temperature PL of the V300 samples is centered at 1.30 μm ,⁴² demonstrating the possibility to reach the technologically important 1.3 μm spectral window with nominally binary InAs/GaAs QD's. Additionally, the growth is highly reproducible: Nominally identical V300 samples (dubbed V300 and V300') grown ~ 8 months apart show a very similar PL with peak energies only 4 meV apart. Figure 1 depicts the PL of the sample V300' on a logarithmic scale showing two characteristic fea-

tures of the investigated samples. First, most samples show a weak but extended high-energy shoulder at low excitation densities, which can be attributed to ground state PL of smaller QD's. AFM results reveal for such samples a size distribution skewed towards smaller islands as a result of the formation process.¹¹ Second, the weak modulation in the low energy slope of the QD PL peak is due to phonon-assisted exciton recombination, which has been studied in detail recently.⁴¹

For the investigated samples with widely varying average QD size the PL yield is practically constant at low excitation densities,^{11,41} suggesting nonradiative recombination to be negligible. Cross-sectional TEM images show that less than $\sim 2\%$ of the islands in the V300 samples (having the largest islands) are dislocated, whereas no dislocations are observed for the other samples. Additionally, AFM investigations show a tendency for the island uniformity to improve with decreasing recombination energy, i.e., with increasing average QD size.¹¹ The improving uniformity is reflected in a decreasing full width at half maximum (FWHM) of the ground state PL peak, which might also benefit from a decreasing quantum size dependence with increasing QD size.¹¹ Correspondingly, the V300 samples show the PL peak with the narrowest FWHM, being, e.g., for sample V300' only 18 meV. As demonstrated below, such samples, combining a high material quality with a high QD uniformity, provide access to the quantum-size effect of the excited state spectrum of self-organized QD's. In contrast to the case of colloidal InAs QD's,³ for which the radius is to a good approximation the dominant free parameter, size, shape, and composition fluctuations provide for an at least three-dimensional parameter space in the case of self-organized InAs/GaAs QD's,²⁰ making detailed investigations of the excited state spectrum difficult.

The excited state spectrum of self-organized QD's is commonly investigated in high-density PL spectra^{6,19,21} taking advantage of state filling. The high-density PL spectrum of the V300' sample (Fig. 1) shows four additional peaks on the high-energy side of the ground state transition with an almost equidistant spacing of ~ 70 meV due to excited state transitions. However, such experiments probe *highly populated* QD's for which many-particle effects need to be taken into account.^{43,44} The relevance of such results for a comparison to calculations of single-exciton states is therefore limited. Furthermore, the high-density PL measurements are bound to the inhomogeneous broadening of the QD ensemble.

A powerful tool for the investigation of the excited state absorption spectrum of empty QD's, circumventing at least part of the inhomogeneous broadening, is PLE spectroscopy.^{3,20,36} The PLE spectrum of the PL maximum of the V300' sample (thick line in Fig. 1) provides information on the excited state transitions, carrier relaxation processes, and the wetting layer (WL). The heavy and light hole absorption of the WL lead to excitation resonances at 1.445 and 1.49 eV. These transition energies are typical for the employed growth conditions and correspond to an ~ 1 -ML-thick InAs quantum well.⁴⁵ Altering the InAs deposition or growing the optically active QD's on a seed layer (as for the V samples) only marginally affects the WL transition energies. Thus, the variation of the QD ground state transition

energy in the investigated samples corresponds directly to the change of the exciton localization energy with respect to the WL, ranging from 270 meV for the C174 sample to 430 meV for the V300 samples. Below 1.4 eV a series of well-resolved excitation resonances is observed, which corresponds to localized excitations of the QD's. The excitation resonances form groups which roughly correspond to the inhomogeneously broadened excited state transitions observed in high-density PL spectra. However, the interpretation of such PLE spectra has been the subject of intensive discussions recently.

The observation of a PLE signal requires a two-step process. First, an exciton is generated in an excited QD state by absorption and, second, this exciton has to relax to the luminescent ground state to generate a measurable signal. Consequently, restricted relaxation processes in 0D systems^{37,38} might prevent PLE spectra to mirror the absorption spectrum. Interlevel relaxation times of some 10 to 100 ps have been deduced from time-resolved PL measurements on self-organized III-V QD's.^{39,46,47} Such slow relaxation processes have to compete with radiative⁴⁰ and nonradiative⁴⁸ recombination processes, which might modify the shape of the PLE spectra. Indeed, PLE spectra reported for self-organized InAs/GaAs QD's are so far mostly dominated by LO-phonon-related resonances,^{39,40,48,49} providing information on the relaxation processes rather than on the excited state spectrum. The fact that at low temperatures and low excitation densities only ground state emission is observed (Fig. 1) might be the result of the details of the intradot relaxation cascade. We will show in the next section that at least for the larger of the QD's studied here this constraint does not apply.

A. Temperature-dependent PLE

A slowed-down carrier relaxation in QD's would prevent the formation of a local equilibrium state, i.e., carriers would recombine from a hot carrier distribution. The carrier distribution in the QD's can be probed at elevated temperatures. The dashed spectrum in Fig. 2(a) shows the nonresonantly excited PL of the V300 sample at 190 K. The spectrum reveals a high-energy shoulder at 1.064 eV attributed to inhomogeneously broadened excited states PL. The thermal population of these excited states can be directly proven in Anti-Stokes PL experiments in which the excitation energy is smaller than the detection energy. In this case, excitons are excited, e.g., in the ground state and subsequently have to absorb phonons to populate the excited states detected in PL. The solid lines in Fig. 2(a) show PL and PLE spectra which have been, respectively, excited and detected at the maximum of the inhomogeneously broadened ground state transition ($E_{\text{exc}} = 0.990$ eV). For the PL and PLE spectra the roles of excitation and detection are just reversed. Both spectra probe the same subensemble of QD's and reveal the same resonances, whereby the large discrepancy of the intensities results from the low thermal population of the excited states in the anti-Stokes PL case. The intensity ratio between the PL and PLE spectra [Fig. 2(b)] is well fitted by a Boltzmann distribution yielding an effective temperature of (175 ± 10) K, which is in good agreement with the nominal sample temperature of 190 K. Obviously, at this temperature, inelastic phonon scattering is much faster than recombination

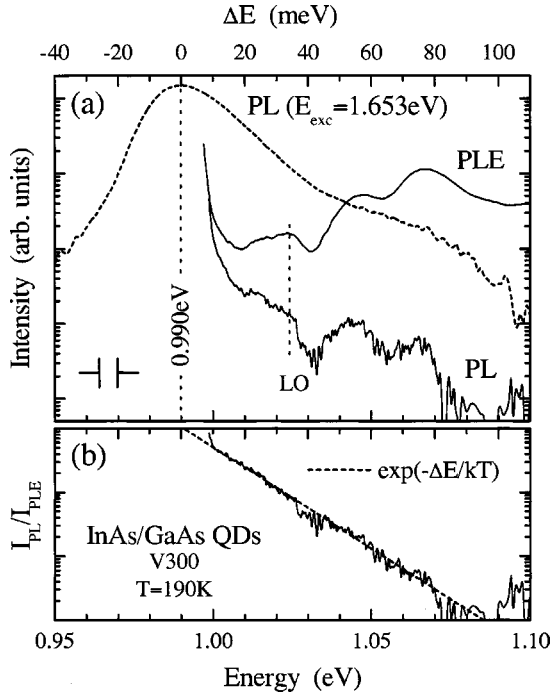


FIG. 2. (a) PL and PLE spectra of the V300 sample at 190 K. The dashed spectrum shows the nonresonantly excited PL and solid lines show anti-Stokes PL and PLE spectra excited and detected, respectively, at the maximum of the inhomogeneous PL peak (0.990 eV). (b) Intensity ratio of the resonant PL and PLE spectra shown in (a). The dashed line shows a Boltzmann fit yielding an exciton temperature of (175 ± 10) K in the QD's. The combined experimental resolution is shown in the lower left corner of (a).

establishing an equilibrium distribution of excitons in the QD's, which is the precondition for PLE spectra to mirror the absorption spectrum. Note that Fig. 2 demonstrates the perfect match ($\Delta E < 1$ meV) of the ground state absorption and emission energies in self-organized InAs/GaAs QD's and, thus, the intrinsic nature of the exciton recombination in the coherent islands.

Carrier relaxation by inelastic phonon scattering is characterized by a temperature-dependent relaxation rate $W_{\text{rel}} \sim [n_B(T) + 1]$, with n_B being the Bose function describing the thermal population of phonon modes. The probability of inelastic phonon scattering processes decreases at lower temperatures,⁴⁶ possibly restricting exciton relaxation at liquid He temperatures. Such restricted exciton relaxation would inevitably alter the shape of the PLE spectra when the sample temperature changes. This effect is, however, *not* observed here, as can be seen in Fig. 3 which shows PLE spectra of sample V300 measured at various temperatures for the respective PL maximum. The shape of the near-resonant excitation is practically unchanged between 5 and 250 K, suggesting exciton scattering between the different localized states in the QD to be faster than radiative and nonradiative recombination processes also at low temperatures. The decreasing relative excitation efficiency for $\Delta E > 200$ meV at the highest sample temperatures is attributed to thermal escape of carriers from excited QD states.^{20,42} Hence, low-temperature PLE spectroscopy is indeed an appropriate size-selective probe of the excited state absorption spectrum of the QD's in the investigated samples.

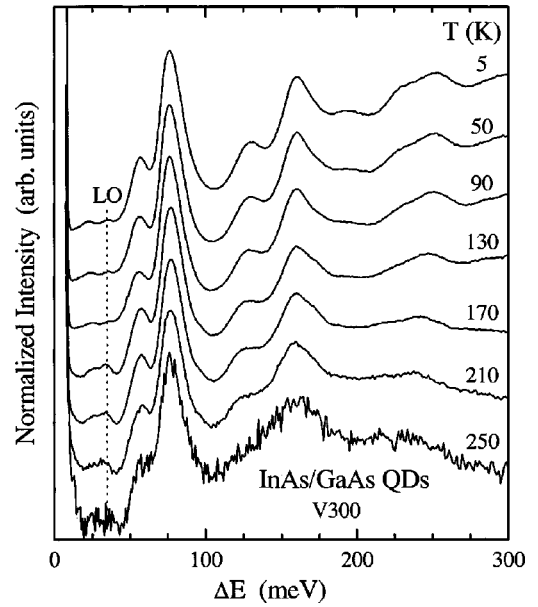


FIG. 3. PLE spectra of the V300 sample at various temperatures as a function of the excess excitation energy. The PLE spectra have been recorded on the temperature-dependent PL maximum.

B. Size-dependent PLE

Figure 4 compares PLE spectra for some of the investigated samples detected near the maximum of the respective ground state PL peak. The spectra are normalized and the energy axis refers to the respective detection energy, thus showing the *excess* excitation energy $\Delta E = E_{\text{exc}} - E_{\text{det}}$. The PLE spectra of the different samples are qualitatively similar. The PLE efficiency is very weak for $\Delta E < 40$ meV. Nevertheless, two weak resonances at ~ 22 and ~ 34 meV are clearly resolved in the PLE spectra (see Fig. 1 and Fig. 2 for logarithmic plots). The latter resonance is found in all

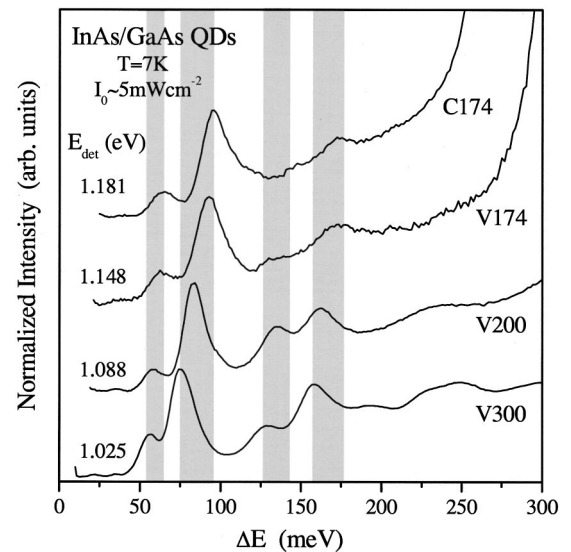


FIG. 4. Normalized PLE spectra of InAs/GaAs QD's for some of the investigated samples as a function of the excess excitation energy ($\Delta E = E_{\text{exc}} - E_{\text{det}}$). The spectra have been detected near the maximum of the respective ground state PL. The various excitation resonances have FWHM's > 10 meV, which are not limited by the experimental resolution (< 4 meV).

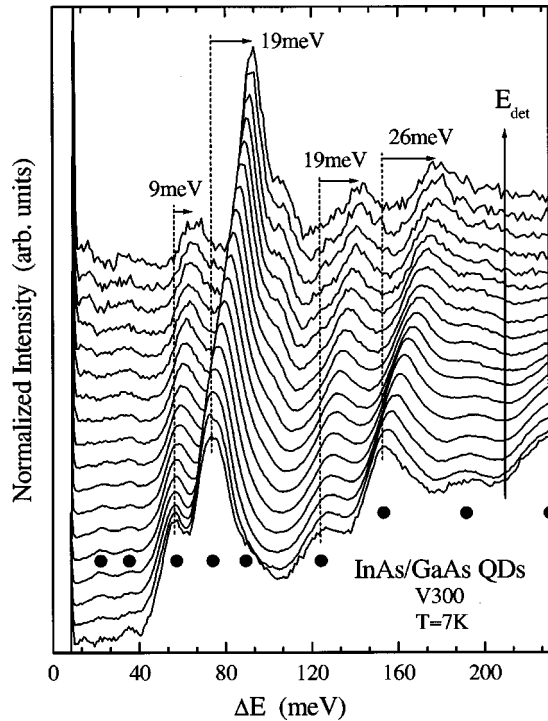


FIG. 5. Normalized PLE spectra of the V300 sample taken at $T=7$ K. The detection energy has been varied in 5 nm steps between 1.012 and 1.088 eV. The dots mark the excitation resonances summarized in Fig. 7.

samples, and attributed to LO-phonon-assisted generation of excitons in the QD ground state.⁴¹ At higher energies two pairs of excitation resonances are observed with components at ~ 60 and ~ 85 meV as well as ~ 135 and ~ 170 meV, respectively, marked by the gray fields in Fig. 4. Additional but less modulated resonances are observed at higher energies for the larger QD's (V200 and V300) providing sufficient exciton localization. The FWHM of the excitation resonances increases with increasing ΔE , which is attributed to an increasing sensitivity of the higher excited states to shape and composition fluctuations of the islands.²⁰

The PLE spectra of the different samples reveal a trend for the excited state resonance energies to decrease with decreasing detection energy, i.e., increasing average QD size (Fig. 4). The average shape and composition of the islands might, however, vary from sample to sample. PLE experiments allow, on the other hand, investigation of the quantum-size effect of the excited state spectrum for *similar* QD's in one sample by stepping a narrow detection window across the inhomogeneously broadened PL peak. In this case the probed QD subensembles might be assumed to vary in average size for similar shape and composition properties. Figure 5 shows for sample V300 a series of normalized PLE spectra at 7 K for detection energies varied in 5 nm steps from 1.012 to 1.088 eV. The excess energy ΔE of the various PLE resonances increases by ~ 9 to ~ 26 meV with increasing detection energy, i.e., decreasing QD size, maintaining the general shape of the PLE spectra.

Figure 6 compares the results of PLE measurements on two samples grown with a 1.74 ML seed layer and different InAs depositions in the optically active second layer (V174 and V300). The PLE intensity at 7 K is given on a logarithmic

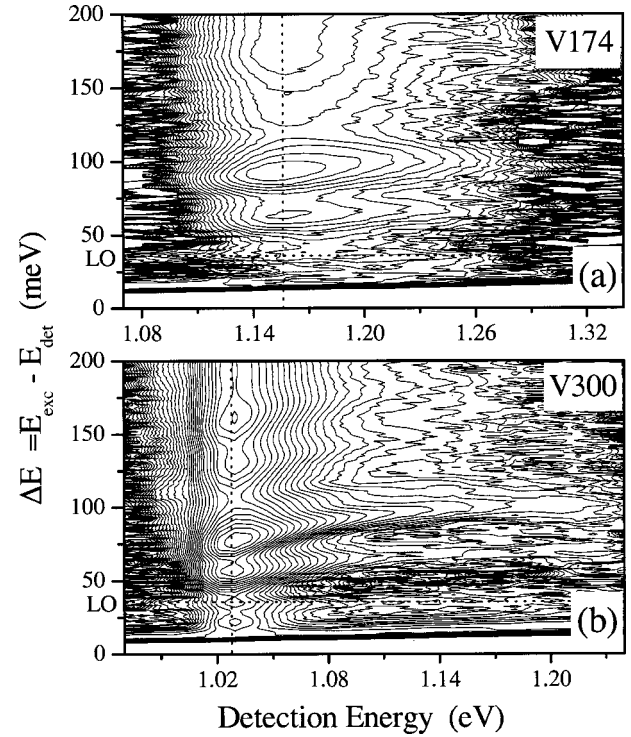


FIG. 6. Contour plots of the PLE intensity in the samples (a) V174 and (b) V300 as a function of the detection energy and the excess excitation energy $\Delta E = E_{exc} - E_{det}$. The intensity is given on a logarithmic scale with the contour lines separated by a factor of 1.25.

mic scale in a contour plot as a function of the detection energy E_{det} and the excess excitation energy ΔE . The respective PL maxima for nonresonant excitation are marked by the vertical dotted lines. The quantum-size effect is clearly observable for sample V300 [Fig. 6(b)] but is negligible for sample V174 [Fig. 6(a)]. Note that for the V300 sample the dominant excitation resonance, observed at excess energies ΔE between 65 and 90 meV, is most intense in the energy gap between the two- and three-LO-phonon processes observed earlier,³⁹ supporting the identification of the excitation resonances with excited state transitions.

Figure 7 compiles the excess excitation energies observed for the dominant PLE resonances (marked by solid dots in Fig. 5) in some of the investigated samples. The most intense excitation resonances appear around excess energies ΔE of ~ 80 , ~ 160 , and ~ 240 meV, roughly corresponding to the excited state transitions observed in inhomogeneously broadened high-density PL (compare with Fig. 1). Additional weaker resonances are resolved at ~ 22 , ~ 60 , ~ 110 , ~ 130 , and ~ 190 meV. Line shape fits to the PLE spectra show additional substructures for some of the resonances which has been omitted in Fig. 7 for the sake of clarity. The excited state transition spectrum of the QD's is, therefore, denser than expected from the inhomogeneously broadened PL spectra. Figure 8 depicts for some resonances in the V300 sample the change of ΔE as a function of the detection energy with respect to that observed for a detection energy of 1.029 eV, close to the maximum of the PL peak. The slopes are clearly different, demonstrating their different electronic origin. The size-selective PLE spectra demonstrate unam-

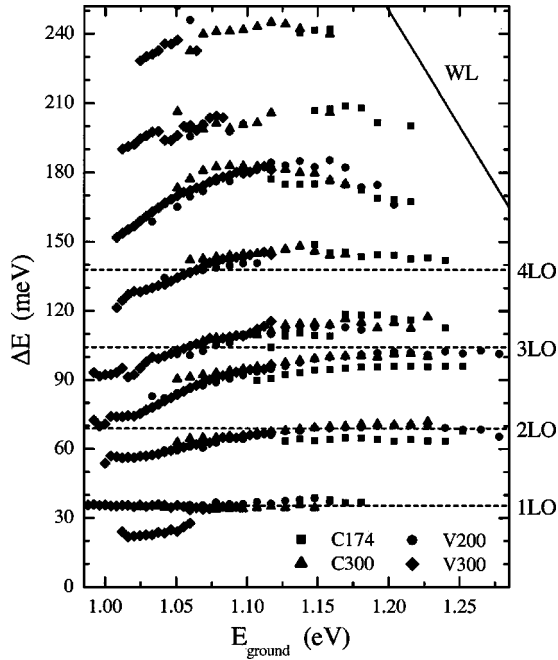


FIG. 7. Peak energies of the excitation resonances observed for the investigated samples. The dotted lines indicate the LO-phonon ladder (Ref. 39).

biguously the quantum-size effect for large self-organized InAs/GaAs QD's with ground state transition energies below ~ 1.1 eV.

For the smaller QD's ($E_{\text{det}} \geq 1.1$ eV) the excitation resonances are *less* dependent on the detection energy. Partly even a reversed size dependence, i.e., an increasing excess excitation energy with increasing QD size, is observed. Previous results for stacked QD's suggest that the observation of a quantum-size dependence requires highly uniform QD's.²⁰

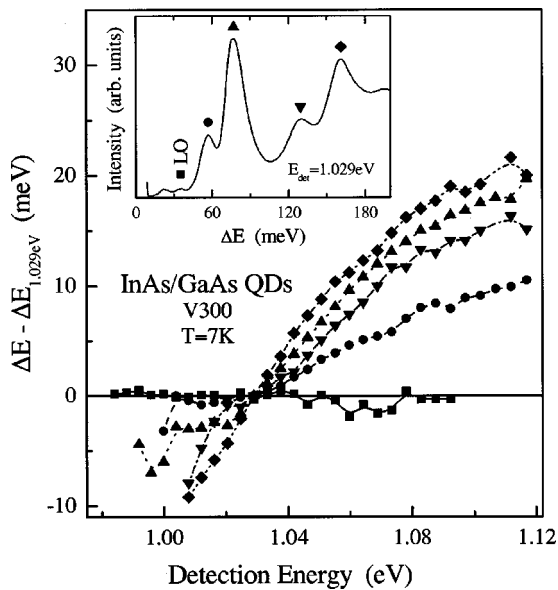


FIG. 8. Change of ΔE of the excitation resonances as a function of the detection energy for the V300 sample. The values are given with respect to the energies observed detecting at 1.029 eV. The inset shows the PLE spectrum detected at 1.029 eV together with the symbols used in the main part of the figure.

The evolution of the excited state spectrum shown in Fig. 7 most likely depends on both the quantum-size effect and on changes in the average island shape and, perhaps, composition.¹⁰ Hence the following discussion is restricted to the samples with 3.00 ML InAs deposition, providing the largest QD's and showing a clear quantum-size effect.

IV. PREDICTED ABSORPTION SPECTRA

The shape and composition of islands formed in the Stranski-Krastanow growth mode are still a controversial topic in literature, especially in the case of overgrown structures for which In segregation and interdiffusion might occur during the growth of the cap layer. Such discrepancies reflect on the one hand the different growth conditions modifying the surface kinetics, and on the other hand the present limitations of commonly available structural characterization techniques. The lack of detailed information on the structural parameters of the islands and, equally important, on their statistical distribution, is still a severe barrier for *fully* justified comparisons with detailed model calculations.

For the investigated samples, special attention has been paid to the growth of the GaAs cap layer in order to minimize the effects of segregation and interdiffusion. The InAs islands were capped at a low substrate temperature of 400 °C using migration enhanced epitaxy, providing high-quality GaAs at such low temperature.³⁶ The combination of AFM and cross-sectional TEM results on an equivalent uncapped V300 sample indicates islands with average base length $b \sim 19$ nm and an aspect ratio suggesting $\{101\}$ side facets. The experimental results might therefore be compared to calculations assuming ideal pyramidal InAs/GaAs QD's with $\{101\}$ side facets available in the literature.^{25–27}

The following discussion is based on the eight-band $\mathbf{k} \cdot \mathbf{p}$ calculations of the single-particle level structure reported by Stier, Grundmann, and Bimberg.²⁶ Coherently strained InAs/GaAs pyramids with base lengths b between 10.2 and 20.4 nm were treated based on experimental values for the required bulk material Γ -point band structure parameters ($T = 6.5$ K). For a comparison with the optical spectra probing correlated electron-hole (exciton) states in the QD's these calculations are extended here to include Coulomb effects on the entire absorption spectrum rather than the ground state transition only. For the sake of clarity we neglect the exchange interaction: The exciton fine structure caused by the exchange interaction is at least one order of magnitude smaller than the experimental resolution of the PLE experiments.⁵⁰ The calculation of the exciton states is based on a multiconfiguration interaction scheme using the set of all available single-particle eigenstates, as described in Appendix A.

The calculations predict ten bound conduction band (CB) and at least eight bound valence band (VB) states in an InAs pyramid with $b = 17$ nm,⁵¹ each of which is only spin degenerate. The low confinement symmetry (ideally C_{2v} due to the atomistic properties and the piezoelectric effect) in such QD's has severe consequences on the electronic eigenstates and on the observable optical transitions: Any *orbital* degeneracy of bound states is removed and, in principle, transitions between all VB and all CB states are allowed, providing for complex absorption spectra. However, only a limited number

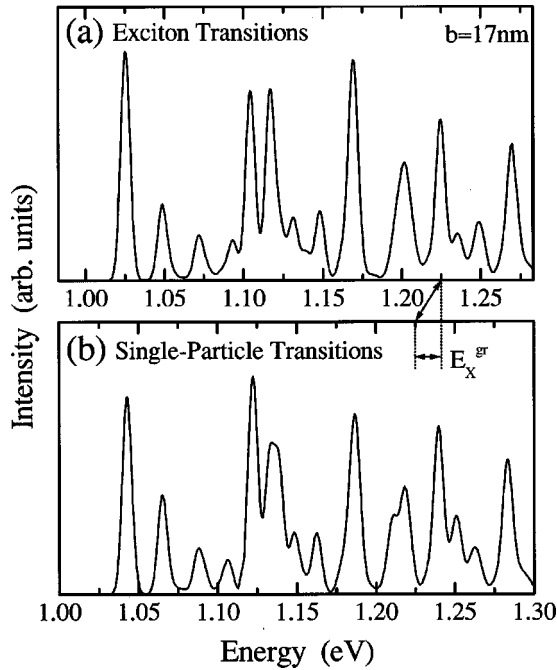


FIG. 9. Absorption spectra calculated for an InAs pyramid ($b = 17$ nm) (a) with and (b) without Coulomb interaction. An inhomogeneous broadening of 7 meV FWHM was assumed. Note that the energy scales of (a) and (b) are shifted by the ground state exciton binding energy E_X^{gr} of 17.3 meV.

of transitions has sufficient oscillator strength to be observed in, e.g., PLE experiments, as can be seen in Fig. 9. Figures 9(a) and 9(b) depict predicted exciton and single-particle absorption spectra assuming an inhomogeneous broadening of 7 meV. The Coulomb interaction, being characteristic for each combination of an electron and hole state, leads to a low-energy shift of the whole absorption spectrum by about one exciton binding energy, slightly modifying the energy separations and the respective transition probabilities.

The predicted absorption spectra in Fig. 9 demonstrate the difference between all-numerical calculations for strained low-symmetry QD's and the equally spaced transitions expected from harmonic oscillator models: A host of absorption lines is predicted rather than single distinct transitions to be labeled by one common quantum number for multiply degenerate CB and VB states. The transitions form, however, *groups* which can be related to the quantum numbers of CB states [compare Fig. 11(a)], owing to the facts that the level separations of the electrons are up to ~ 3 times larger than those of the holes and that the C_{2v} splitting of the electron levels is small compared to the quantization energies. In contrast, the hole states can no longer be traced back to fictitious two-dimensional harmonic oscillator states.

The physical reason for the lack of elementary dipole selection rules and the nontrivial polarization properties of dipole transitions are strong *band mixing* effects which are caused by the confinement in general and enhanced by its high dimension and low symmetry, and by strain effects. The majority of zero-dimensional hole states cannot be properly classified as ‘‘light’’ or ‘‘heavy’’ which also causes the loss of *parity*. For a pyramidal InAs/GaAs QD only the index n of each state, obtained by sorting all states by their energies, remains a good quantum number. The number of the domi-

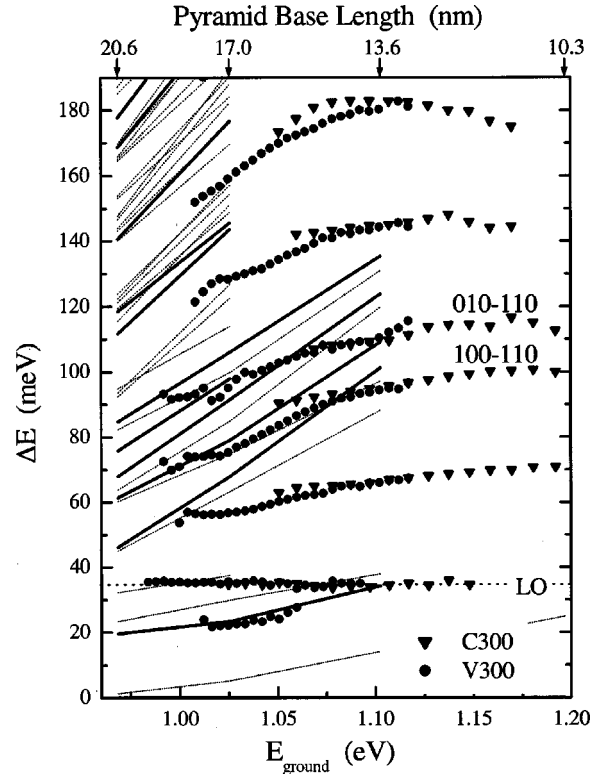


FIG. 10. Peak energies of the excitation resonances of the QD ground state PL in the 3.00 ML samples (C300 and V300). Lines represent results of eight-band $\mathbf{k} \cdot \mathbf{p}$ calculations for pyramidal InAs/GaAs QD's with $\{101\}$ side facets. Thick lines correspond to transitions with at least 10% of the oscillator strength of the ground state transition. Thin lines show weaker transitions.

nant envelope function's nodal surfaces tangential to one of the three basic symmetry planes of the QD [$(1\bar{1}0)$, (110) , and (001)] may, however, be used for labeling purposes.²⁶ Such labeling works for the lowest QD states but tends to fail for highly excited VB states, where the enhanced band mixing completely smears out the nodal surfaces in the probability density.

V. DISCUSSION

In order to gain more insight into the electronic origin of the transitions observed in PLE spectra we compare in Fig. 10 the experimental results for the samples grown with 3.00 ML InAs deposition to the eight-band $\mathbf{k} \cdot \mathbf{p}$ calculations for ideal InAs pyramids. Thick solid lines represent calculated transitions having at least 10% of the maximum intensity. Thin dotted lines show the remaining weaker transitions. The predictions are in qualitative agreement with the experimental observations in case of the larger islands ($E_{\text{det}} \leq 1.1$ eV), predicting excited state absorption in the energy region for which PLE spectra show excitation resonances. The predicted level separations for a given ground state transition energy E_{det} are, however, systematically larger than experimentally observed.

Indeed for a given pyramid base length the calculations predict the ground state transition energy ~ 40 meV below the experimental value.⁴¹ Possible origins for this discrepancy will be discussed in more detail below. Taking the

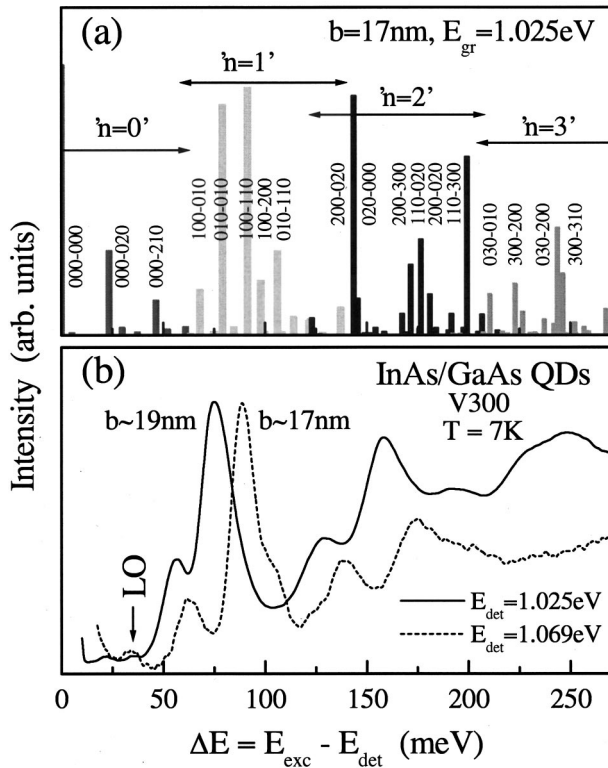


FIG. 11. Comparison between calculated absorption and experimental PLE spectra. (a) Calculated transitions are represented by bars with a height corresponding to the relative oscillator strength for $b = 17$ nm. (b) PLE spectra of sample V300 for detection energies of 1.025 eV, corresponding to the *calculated* ground state transition energy for $b = 17$ nm, and of 1.069 eV, for which the estimated base length of ~ 17 nm corresponds to that of the calculated pyramid.

pyramid base length as reference, i.e., adding ~ 40 meV to the calculated ground state transition energy, would significantly improve the agreement of the predicted excited state transition spectrum to the experimental data in Fig. 10. A more detailed comparison is given in Fig. 11. Figure 11(a) depicts the calculated single-exciton absorption spectrum for $b = 17$ nm, whereby each transition is represented by a bar with a length corresponding to its relative oscillator strength. The agreement with PLE spectra detected at the predicted ground state transition energy of 1.025 eV is only qualitative [solid spectrum in Fig. 11(b)]. Better agreement is, however, found for PLE spectra detected at 1.069 eV [dashed spectrum in Fig. 11(b)] for which the estimated QD base length of ~ 17 nm (Ref. 41) matches the *size* of the calculated pyramid.

In view of the uncertainties regarding the actual island shape and composition in the samples, as well as some of the material parameters entering the calculations, the agreement is fairly remarkable. The discrepancy between the experimental and calculated ground state transition energy could be improved by including the nonlinear strain dependence of the bulk band gap⁵² or using bulk bandstructure parameters, which rather approximate the relevant near Γ -point part of the Brillouin zone than the Γ point itself. However, doing such adjustments based on the experimental results would be speculative at the present state. For example, *interdiffusion* might contribute to the observed discrepancies too: Interdif-

fusion decreases the confinement depth and increases the effective QD size, which elevates the exciton ground state energy and reduces the excited state separation, respectively.⁵³

The applicability of the eight-band $\mathbf{k} \cdot \mathbf{p}$ calculations to the interpretation of experimental results for self-organized InAs/GaAs QD's is also supported by recent investigations of the polar exciton-LO-phonon coupling.⁴¹ The polar exciton-LO-phonon coupling depends sensitively on the actual electron and hole part of the exciton wave function, making the coupling strength a probe of the three-dimensional shape of the confinement potential, e.g., of the C_{2v} contribution. The experimentally observed coupling strength is well described by the eight-band $\mathbf{k} \cdot \mathbf{p}$ calculations for $\{101\}$ faceted pyramidal InAs/GaAs QD's including the piezoelectric effect, thus indicating that the assumed ideal island shape and composition are reasonable approximations for the investigated QD's.

Another equally important test for the material parameters used in the model calculations is the splitting of the exciton localization energy between the CB and VB, i.e., the single-particle level positions with respect to the barrier (GaAs) band edges. Such information is only indirectly accessible in optical spectroscopy of exciton transitions but can be derived from capacitance spectroscopy. Recent investigations of electron and hole localization energies in self-organized InAs/GaAs QD's by deep level transient spectroscopy were found in good agreement with predictions, supporting the present $\mathbf{k} \cdot \mathbf{p}$ model to provide a good approximation to the electronic structure of such QD's.^{54,55}

Figures 10 and 11 allow for a tentative assignment of the observed excitation resonances to single-exciton transitions based on their energy and relative intensity. The temperature-dependent results (Figs. 2 and 3) show that the luminescence detected in the PLE experiments originates from the ground state exciton recombination. As outlined in the Appendix, the exciton transitions may still be classified by the dominating single-particle contributions, which are $|C000\rangle$ and $|V000\rangle$ for the ground state. Corresponding identification of the dominant contributions to the excited exciton states are given in Fig. 11(a) for transitions having at least 10% of the intensity of the oscillator strength of the ground state transition.

A comparison of Figs. 11(a) and 11(b) suggests that the excitation resonance at ~ 22 meV, exhibiting a slight blue-shift with decreasing QD size (Fig. 10), corresponds to the exciton transition involving $|C000\rangle$ and the second excited VB state $|V020\rangle$, which has two "nodes" in the $[110]$ direction. The resonances between 50 and 120 meV are attributed to transitions from different VB states to the lowest excited CB states $|C100\rangle$ and $|C010\rangle$, being split by the C_{2v} -potential contribution. Figure 12 depicts the energy difference between the $|C100\rangle$ - $|V110\rangle$ and $|C010\rangle$ - $|V110\rangle$ exciton transitions as a function of the ground state transition energy. The splitting increases with increasing QD size in contrast to the expected quantum-size effect. Indeed, such an "inverse" size dependence is expected from the piezoelectric contribution to the C_{2v} potential. The eight-band $\mathbf{k} \cdot \mathbf{p}$ calculations (open circles) predict the correct slope of the splitting but underestimate the magnitude. The asymmetry due to the atomistic inequivalence of the $(1\bar{1}0)$ and (110) directions as well as the underestimation of the ground state

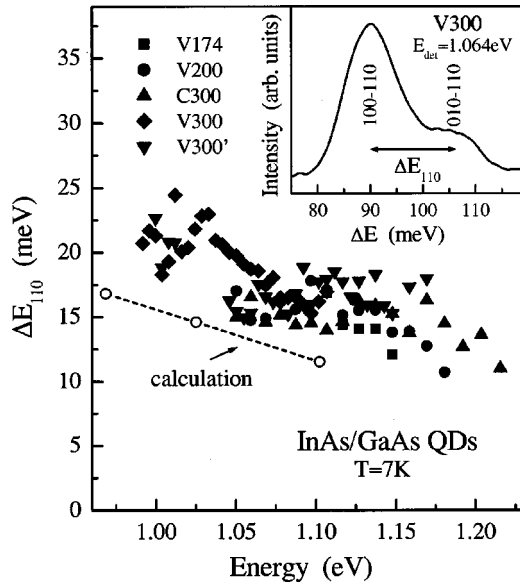


FIG. 12. Energy splitting of the $|C100\rangle$ - $|V110\rangle$ and $|C010\rangle$ - $|V110\rangle$ exciton transitions as a function of the ground state transition energy. The inset depicts the corresponding excitation resonances for the V300 sample.

transition energy might account for the remaining discrepancy.^{26,27}

The resonances in the ΔE range between 130 and 210 meV are attributed to transitions from the $|V000\rangle$, $|V020\rangle$, and $|V300\rangle$ hole states to the generically degenerate states $|C200\rangle$, $|C020\rangle$, and $|C110\rangle$. These *line groups* approximately resemble the quantized levels of the two-dimensional harmonic oscillator (labeled $n=0,1,2, \dots$) being ideally $(n+1)$ -fold degenerate (neglecting spin). In fact, the given assignment captures only the *main* contributions to the various transitions. As is obvious from Fig. 11(a) a much richer fine structure is predicted, which for the present samples is, however, still masked by inhomogeneous broadening. The large FWHM (>10 meV, attributed to shape and/or composition fluctuations) of the PLE resonances renders a more detailed identification meaningless. Finally, Fig. 11 suggests that the fading fine structure of the PLE spectra with increasing ΔE is due to the increasing density of exciton transitions, which makes it harder to resolve individual transitions.

As already observed, the calculations fail to explain the PLE spectra of the smaller QD's ($E_{\text{det}} \geq 1.1$ eV). The observed energy separations are significantly smaller than predicted and seemingly lack any size dependence (Fig. 7). On the one hand, the limitations of $\mathbf{k} \cdot \mathbf{p}$ theory to describe the band structure for large k vectors might cause significant overconfinement for highly excited states or small QD's. On the other hand, the excitation resonances at large detection energies seem to assume a ladder corresponding to multiples of LO-phonon energies (Fig. 7). A possible explanation might be slower relaxation and more efficient interaction with nonradiative recombination centers in the barrier for the smaller QD's.³⁹ Additionally, less structural information exists for the smaller islands, and shape and composition changes (e.g., due to interdiffusion) are expected to play a more important role for smaller QD's.

Finally, the higher excited resonances show an inverse size dependence, i.e., ΔE decreases with increasing detection

energy, when the transition energy approaches that of the WL (Fig. 7). Coulomb interaction between carriers localized in the QD's and their two-dimensional opposite in the WL results in localized exciton states. Pinning of the energy of the two-dimensional carrier to the WL would then force an inverse size dependence of the optical transition energy for a certain detection energy range. Unfortunately, our calculations do not account for interactions between localized and two-dimensional carriers.

The above discussion of the optical properties of self-organized InAs/GaAs QD's based on the eight-band $\mathbf{k} \cdot \mathbf{p}$ (envelope function) method demonstrates a reasonable predicting capability of the model, concerning both the energy and wave function of the localized states for a given lateral QD size. The applicability of envelope function theory to such small strained QD's has, however, been questioned, recently.²⁷ Indeed, significantly different electronic and optical properties have been predicted for pyramidal InAs/GaAs QD's based on atomistic empirical pseudopotential (EP) calculations. Exciton ground state energies between 1.28 and 1.00 eV have been obtained for QD base lengths of $4 \leq b \leq 9$ nm,²⁷ whereas our $\mathbf{k} \cdot \mathbf{p}$ calculations require twice as large pyramids ($8 \leq b \leq 18$ nm).²⁶ Additionally, the EP calculations predict for a given ground state transition energy higher excess energies ΔE for the excited state transitions. These significant differences can to a large extent be attributed to the different *bulk band-structure properties* assumed in both calculations.^{26,27} The EP calculations use "close to *ab initio*" pseudopotentials and material parameters derived from corrected LDA calculations,²⁷ whereas the $\mathbf{k} \cdot \mathbf{p}$ calculations employ experimental parameters for the Γ -point band-structure properties.²⁶ The consequences of the fundamental $\mathbf{k} \cdot \mathbf{p}$ approximations^{26,27} are presently negligible for the interpretation of our experimental results, considering the relatively large size of the investigated QD's and the limited accuracy of both the structural information and the bulk band-structure properties.

VI. CONCLUSIONS

For a series of high-quality InAs/GaAs QD samples the excited state transition spectrum was investigated in PLE spectroscopy as a function of the ground state transition energy. Temperature-dependent measurements demonstrate for the larger QD's with a ground state transition energy below ~ 1.1 eV that the observed excitation resonances represent the absorption spectrum of a subset of similar QD's having the same ground state transition energy. The PLE spectra reveal a complex excited state transition spectrum and demonstrate the quantum-size effect of the latter. Energy shifts of excitation resonances of up to ~ 30 meV are observed in a single sample. A detailed comparison with eight-band $\mathbf{k} \cdot \mathbf{p}$ calculations for $\{101\}$ faceted pyramidal InAs/GaAs QD's shows good qualitative agreement, enabling a tentative assignment of the excitation resonances. An increasing deviation between the predicted and observed optical properties for smaller QD's is attributed to an increasing discrepancy between the assumed and actual structural properties of the QD's and the barrier as well as to neglecting localized wetting layer states in the calculations.

The experimental investigation of the excited state transi-

tion spectrum of self-organized InAs/GaAs QD's demonstrates the importance of the actual structural properties of such overgrown islands. Model calculations based on the eight-band $\mathbf{k} \cdot \mathbf{p}$ method, which take into account the piezoelectric effect, provide a far reaching understanding of the electronic properties of such low-symmetry strained QD's.

ACKNOWLEDGMENTS

Parts of this work were supported by the US Air Force Office of Scientific Research under the MURI program, and by Deutsche Forschungsgemeinschaft in the framework of Sonderforschungsbereich 296. Parts of the band structure calculation were performed on the Cray T3E-1200LC136/900LC272 of Konrad-Zuse-Zentrum für Informationstechnik Berlin.

APPENDIX: CALCULATION OF EXCITON SPECTRA

The single-exciton spectra [e.g., Fig. 9(a)] are derived from the single-particle spectra calculated in Ref. 26 treating the electrostatic attraction in a multiconfiguration interaction approach taking correlation effects into account. The Coulomb interaction between the electron and hole forming an exciton is calculated using a nonseparable variation ansatz for the exciton wave function $\Psi^{(X)}$. The latter is expanded into a cartesian product basis built from all available 0D electron ($\Psi^{(c)}$) and hole states ($\Psi^{(v)}$):

$$\Psi^{(X)} = \sum_{a,b} \xi_{ab} \Psi_a^{(c)} \Psi_b^{(v)}, \quad (\text{A1})$$

$$\mathbf{p}^{(X)} = \sum_{a,b} \xi_{ab} \mathbf{p}_{ab}. \quad (\text{A2})$$

$\mathbf{p}^{(X)}$ is the dipole term of the absorption due to generation of $\Psi^{(X)}$ and \mathbf{p}_{ab} are the dipole matrix elements of the hypothetical single-particle generations given by Eq. (18) in Ref. 26. Thus the exchange interaction is neglected, and since no magnetic field is considered, each excitonic energy level $|n\rangle$ possesses a four-dimensional orthogonal basis $\{\Psi_{n,1}, \Psi_{n,2}, \Psi_{n,3}, \Psi_{n,4}\}^{(X)}$. The oscillator strength of such a degenerate energy level with light having an electric field vector parallel to the unit vector \hat{e} is obtained by incoherent averaging over the eigenspace

$$|\hat{e} \cdot \mathbf{p}_n^{(X)}|^2 = \frac{1}{4} (|\hat{e} \cdot \mathbf{p}_{n,1}^{(X)}|^2 + |\hat{e} \cdot \mathbf{p}_{n,2}^{(X)}|^2 + |\hat{e} \cdot \mathbf{p}_{n,3}^{(X)}|^2 + |\hat{e} \cdot \mathbf{p}_{n,4}^{(X)}|^2) \quad (\text{A3})$$

analogous to Eq. (20) in Ref. 26. In the PLE experiments unpolarized, vertically incident excitation was used, hence $\hat{e} \perp [001]$. The intensity I is given by

$$I \propto \int_0^{2\pi} |\mathbf{p}_{[100]} \cos \phi + \mathbf{p}_{[010]} \sin \phi|^2 d\phi \quad (\text{A4})$$

$$= \pi (|\mathbf{p}_{[100]}|^2 + |\mathbf{p}_{[010]}|^2) \quad (\text{A5})$$

$$= 2\pi |\mathbf{p}_{[100]}|^2 \quad (\text{A6})$$

with

$$\mathbf{p}_{[100]} = (1,0,0) \cdot \mathbf{p}_{n,i}^{(X)}, \quad \mathbf{p}_{[010]} = (0,1,0) \cdot \mathbf{p}_{n,i}^{(X)}, \quad i = 1,2,3,4. \quad (\text{A7})$$

I is proportional to the intensity for [100] polarized excitation due to the equivalence of the [100] and [010] directions in [100] oriented pyramidal QD's.

The expansion coefficients ξ_{ab} in Eq. (A1) of all exciton states $|n,i\rangle$ are calculated by the Rayleigh-Ritz algorithm, i.e., diagonalization of the exciton Hamiltonian $H^{(X)}$ over the entire Cartesian basis:

$$H^{(X)} = H_c - H_v - \frac{e^2}{4\pi\epsilon_0} \frac{1}{\epsilon_r(\mathbf{r}_c, \mathbf{r}_v)} \frac{1}{|\mathbf{r}_c - \mathbf{r}_v|}, \quad (\text{A8})$$

$$H^{(X)}(\xi_{ab})_{n,i} = E_n^{(X)}(\xi_{ab})_{n,i}, \quad (\text{A9})$$

where H is the single-particle Hamiltonian from Eq. (12) in Ref. 26, e the electron charge, ϵ_0 the vacuum permittivity, ϵ_r the dielectric function of the heterostructure, \mathbf{r} the position operator, and $E^{(X)}$ the excitonic recombination energy. The subscripts c and v denote that the respective operator acts only on the CB or VB part, respectively, of the exciton wave function Eq. (A1). The matrix elements of $H^{(X)}$ are

$$H_{ab,jk}^{(X)} = [E_a^{(c)} - E_b^{(v)}] \delta_{aj} \delta_{bk} - \frac{e^2}{4\pi\epsilon_0} \left\langle \Psi_a^{(c)} \Psi_b^{(v)} \left| \frac{1}{\epsilon_r(\mathbf{r}_c, \mathbf{r}_v) |\mathbf{r}_c - \mathbf{r}_v|} \right| \Psi_j^{(c)} \Psi_k^{(v)} \right\rangle, \quad (\text{A10})$$

where $E_a^{(c)}$ ($E_b^{(v)}$) is the eigenvalue of H belonging to $\Psi_a^{(c)}$ ($\Psi_b^{(v)}$), i.e., the single electron (hole) energy. In the case of the pyramid with $b = 17$ nm the dimension of $H^{(X)}$ is 320, so that 51 360 potentially different matrix elements need to be calculated.⁵¹ Although, in our case, since spin degeneracy yields a reduction it is not recommended to evaluate Eq. (A10) as is, since the calculation of the sixfold integrals is tedious and does not allow for an elegant treatment of the dielectric function ϵ_r . A better way to calculate $H^{(X)}$ is, of course, to use Green's formula and decompose Eq. (A10) into a solution of the Poisson equation (using nested iteration⁵⁶) and a subsequent threefold integral.⁵⁷

$$\nabla[\epsilon_r(\mathbf{r}_c) \nabla U^{(c)}(\mathbf{r}_c)] = \frac{e^2}{4\pi\epsilon_0} \Psi_a^{(c)\dagger}(\mathbf{r}_c) \Psi_j^{(c)}(\mathbf{r}_c), \quad (\text{A11})$$

$$H_{ab,jk}^{(X)} = [E_a^{(c)} - E_b^{(v)}] \delta_{aj} \delta_{bk} + \langle \Psi_b^{(v)} | U^{(c)} | \Psi_k^{(v)} \rangle \quad (\text{A12})$$

[the wave function product on the right hand side of Eq. (A11) is a scalar product of two eight-dimensional vectors Eq. (13) in Ref. 26]. Hereby the spatial variation of the dielectric constant ϵ_r , leading to "image charge" effects, is fully taken into account,²⁶ and the possibility to lift the time-reversal degeneracy by the exchange interaction or magnetic fields is left open.

As the approach outlined here is the natural continuation of the eight-band $\mathbf{k} \cdot \mathbf{p}$ single-particle calculations²⁶ it has three advantages: (a) *It is accurate* in the sense that it makes full use of all available information [see also the discussion

of Eq. (18) in Ref. 26]. (b) *It performs rapidly.* (c) *It requires no intuition*, e.g., to find an appropriate variational ansatz.

Since $H^{(X)}$ in Eq. (A9) is not diagonal most of its eigenvectors $(\xi_{ab})_{n,i}$ mix several different electron (a) and hole (b) states into each exciton wave function $\Psi_{n,i}^{(X)}$ in Eq. (A1).

However, in most cases one component (a,b) dominates the degenerate exciton state $|n, i\rangle$ for all i . Hence, the exciton states $|n\rangle$ can still be classified by the dominant CB $|a\rangle$ and VB $|b\rangle$ contributions, thus considering the Coulomb force an *energetic* correction only, see Fig. 9.

- ¹R. Dingle, W. Wiegman, and C. H. Henry, Phys. Rev. Lett. **33**, 827 (1974).
- ²D. J. Norris and M. G. Bawendi, Phys. Rev. B **53**, 16 338 (1996).
- ³U. Banin, C. J. Lee, A. A. Guzelian, A. V. Kadavanich, A. P. Alvisatos, W. Jaskolki, G. W. Bryant, Al. L. Efros, and M. Rosen, J. Chem. Phys. **109**, 2306 (1998).
- ⁴A. Forchel, R. Steffen, T. Koch, M. Michel, M. Albrecht, and T. L. Reinecke, Semicond. Sci. Technol. **11**, 1529 (1996).
- ⁵K. Brunner, U. Bockelmann, G. Abstreiter, M. Walther, G. Böhm, G. Tränkle, and G. Weimann, Phys. Rev. Lett. **69**, 3216 (1992).
- ⁶H. Lipsanen, M. Sopanen, and J. Ahopelto, Phys. Rev. B **51**, 13 868 (1995).
- ⁷For a recent review see, D. Bimberg, M. Grundmann, and N. N. Ledentsov, *Quantum Dot Heterostructures* (Wiley, Chichester, 1999).
- ⁸J. M. Moison, F. Houzay, F. Barthe, L. Leprince, E. André, and O. Vatel, Appl. Phys. Lett. **64**, 196 (1994).
- ⁹N. P. Kobayashi, T. R. Ramachandran, P. Chen, and A. Madhukar, Appl. Phys. Lett. **68**, 3299 (1996).
- ¹⁰I. Mukhametzhano, J. Wei, R. Heitz, and A. Madhukar, Appl. Phys. Lett. **75**, 85 (1999).
- ¹¹I. Mukhametzhano, R. Heitz, J. Zheng, P. Chen, and A. Madhukar, Appl. Phys. Lett. **73**, 1341 (1998).
- ¹²R. Heitz, I. Mukhametzhano, P. Chen, and A. Madhukar, Phys. Rev. B **58**, R10 151 (1998).
- ¹³S. Ruvimov, P. Werner, K. Scheerschmidt, J. Heydenreich, U. Richter, N. N. Ledentsov, M. Grundmann, D. Bimberg, V. M. Ustinov, A. Yu. Egorov, P. S. Kop'ev, and Zh. I. Alferov, Phys. Rev. B **51**, 14 766 (1995).
- ¹⁴G. S. Solomon, M. C. Larson, and J. S. Harris, Appl. Phys. Lett. **69**, 1897 (1996).
- ¹⁵Y. Nabetani, T. Ishikawa, S. Noda, and A. Sasaki, J. Appl. Phys. **76**, 347 (1994).
- ¹⁶M. Tabuchi, S. Noda, and A. Sasaki, in *Science and Technology of Mesoscopic Structures*, edited by S. Namba, C. Hamaguchi, and T. Ando (Springer, Tokyo, 1992), p. 379.
- ¹⁷H. Lee, R. Lowe-Webb, W. Yang, and P. Sercel, Appl. Phys. Lett. **72**, 812 (1998).
- ¹⁸H. Eisele, O. Flebbe, T. Kalka, C. Preinesberger, F. Heinrichsdorff, A. Krost, D. Bimberg, and M. Dähne-Prietsch, Appl. Phys. Lett. **75**, 106 (1999).
- ¹⁹M. Grundmann, N. N. Ledentsov, O. Stier, J. Böhrer, D. Bimberg, V. M. Ustinov, P. S. Kop'ev, and Zh. I. Alferov, Phys. Rev. B **53**, R10 509 (1996).
- ²⁰R. Heitz, A. Kalburge, Q. Xie, M. Grundmann, P. Chen, A. Hoffmann, A. Madhukar, and D. Bimberg, Phys. Rev. B **57**, 9050 (1998).
- ²¹S. Raymond, S. Fafard, P. J. Poole, A. Wojs, P. Hawrylak, S. Charbonneau, D. Leonard, R. Leon, P. M. Petroff, and J. L. Merz, Phys. Rev. B **54**, 11 548 (1996).
- ²²K. Mukai, N. Ohtsuka, H. Shoji, and M. Sugawara, Phys. Rev. B **54**, R5243 (1996).
- ²³S. Noda, T. Abe, and M. Tamura, Physica E (Amsterdam) **2**, 643 (1998).
- ²⁴A. Wojs and P. Hawrylak, Phys. Rev. B **53**, 10 841 (1996).
- ²⁵H. Jiang and J. Singh, IEEE J. Quantum Electron. **34**(7), 1188 (1998).
- ²⁶O. Stier, M. Grundmann, and D. Bimberg, Phys. Rev. B **59**, 5688 (1999).
- ²⁷L.-W. Wang, J. Kim, and A. Zunger, Phys. Rev. B **59**, 5678 (1999).
- ²⁸K. Brunner, G. Abstreiter, G. Böhm, G. Tränkle, and G. Weimann, Phys. Rev. Lett. **73**, 1138 (1994).
- ²⁹M. Notomi, T. Furuta, H. Kamada, J. Temmyo, and T. Tamamura, Phys. Rev. B **53**, 15 743 (1996).
- ³⁰D. Gammon, E. S. Snow, B. V. Shanabrook, D. S. Katzer, and D. Park, Science **273**, 87 (1996).
- ³¹D. Hessman, P. Castrillo, M.-E. Pistol, C. Pryor, and L. Samuelson, Appl. Phys. Lett. **69**, 749 (1996).
- ³²M. Grundmann, J. Christen, N. N. Ledentsov, J. Bhrrer, D. Bimberg, S. S. Ruvimov, P. Werner, U. Richter, U. Gsele, J. Heydenreich, V. M. Ustinov, A. Yu. Egorov, A. E. Zhukov, P. S. Kopev, and Zh. I. Alferov, Phys. Rev. Lett. **74**, 4043 (1995).
- ³³A. Gustafsson, M.-E. Pistol, L. Montelius, and L. Samuelson, J. Appl. Phys. **84**, 1715 (1998).
- ³⁴Y. Toda, S. Shinomori, K. Suzuki, and Y. Arakawa, Phys. Rev. B **58**, R10 147 (1998).
- ³⁵A. Zrenner, M. Markmann, E. Beham, F. Findeis, G. Böhm, and G. Abstreiter, J. Electron. Mater. **28**, 542 (1999).
- ³⁶Q. Xie, P. Chen, A. Kalburge, T. R. Ramachandran, A. Nayfonov, A. Konkar, and A. Madhukar, J. Cryst. Growth **150**, 357 (1995).
- ³⁷H. Benisty, C. M. Sotomayor-Torres, and C. Weisbuch, Phys. Rev. B **44**, 10 945 (1991).
- ³⁸T. Inoshita and H. Sakaki, Phys. Rev. B **46**, 7260 (1992).
- ³⁹R. Heitz, M. Veit, N. N. Ledentsov, A. Hoffmann, D. Bimberg, V. M. Ustinov, P. S. Kop'ev, and Zh. I. Alferov, Phys. Rev. B **56**, 10 435 (1997).
- ⁴⁰M. J. Steer, D. J. Mowbray, W. R. Tribe, M. S. Skolnick, M. D. Sturge, M. Hopkinson, A. G. Cullis, C. R. Whitehouse, and R. Murray, Phys. Rev. B **54**, 17 738 (1996).
- ⁴¹R. Heitz, I. Mukhametzanov, O. Stier, A. Madhukar, and D. Bimberg, Phys. Rev. Lett. **83**, 4654 (1999).
- ⁴²R. Heitz, I. Mukhametzanov, A. Madhukar, A. Hoffmann, and D. Bimberg, J. Electron. Mater. **28**, 520 (1999).
- ⁴³L. R. Fonseca, J. L. Jimenez, J. P. Leburton, and R. M. Martin, Phys. Rev. B **57**, 4017 (1998).
- ⁴⁴A. Wojs and P. Hawrylak, Solid State Commun. **100**, 487 (1996).
- ⁴⁵R. Heitz, T. R. Ramachandran, A. Kalburge, Q. Xie, I. Mukhametzhano, P. Chen, and A. Madhukar, Phys. Rev. Lett. **78**, 4071 (1997).
- ⁴⁶B. Ohnesorge, M. Albrecht, J. Oshinowo, A. Forchel, and Y.

- Arakawa, Phys. Rev. B **54**, 11 532 (1996).
- ⁴⁷S. Grosse, J. H. H. Sandmann, G. von Plessen, J. Feldmann, H. Lipsanen, J. Tulkki, and J. Ahopelto, Phys. Rev. B **55**, 4473 (1997).
- ⁴⁸R. Heitz, M. Grundmann, N. N. Ledentsov, L. Eeckey, M. Veit, D. Bimberg, V. M. Ustinov, A. Yu. Egorov, A. E. Zhukov, P. S. Kop'ev, and Zh. I. Alferov, Appl. Phys. Lett. **68**, 361 (1996).
- ⁴⁹K. H. Schmidt, G. Medeiros-Ribeiro, M. Oestereich, P. M. Petroff, and G. H. Döhler, Phys. Rev. B **54**, 11 346 (1996).
- ⁵⁰O. Stier, A. Schliwa, R. Heitz, M. Grundmann, and D. Bimberg, Phys. Status Solidi B (to be published).
- ⁵¹In Ref. 26 the highly excited electron states $|020\rangle$, $|300\rangle$, $|001\rangle$, and $|011\rangle$ in the $b=17.0$ nm QD are erroneously missing. Thus not six but ten bound CB states are predicted for these QD's.
- ⁵²G. H. Li, A. R. Goni, C. Abraham, K. Syassen, P. V. Santos, A. Cantarero, O. Brandt, and K. Ploog, Phys. Rev. B **50**, 1575 (1994).
- ⁵³F. Heinrichsdorff, M. Grundmann, O. Stier, A. Krost, and D. Bimberg, J. Cryst. Growth **195**, 540 (1998).
- ⁵⁴C. M. A. Kapteyn, F. Heinrichsdorff, O. Stier, R. Heitz, M. Grundmann, N. D. Zakharov, D. Bimberg, and P. Werner, Phys. Rev. B **60**, 14 265 (1999).
- ⁵⁵C. M. A. Kapteyn, M. Lion, R. Heitz, D. Bimberg, P. Brunkov, B. V. Volovik, S. G. Konnikov, A. R. Kovsh, and V. M. Ustinov, Appl. Phys. Lett. **76**, 1573 (2000).
- ⁵⁶W. H. Press, B. P. Flannery, S. A. Teukolsky, and W. T. Vetterling, *Numerical Recipes in C*, 2nd ed. (Cambridge University Press, Cambridge, 1992).
- ⁵⁷In Eqs. (A11) and (A12) the roles of the CB and VB parts can be interchanged, of course.